WA-DED SPECIFIC TOPOLOGY OPTIMIZATION OF A KINGPIN PLATE FOR SEMI-TRAILERS

F. HAUNREITER*, M. SILMBROTH*, K. BHARADWAJ*, H. DREXLER*, M. SCHWENDINGER**, H. BRUHNS**, A. BAUER**

**LKR Light Metals Technologies GmbH, AIT Austrian Institute of Technology, 5282 Ranshofen, Austria*
***Wilhelm Schwarzmüller GmbH, 4785 Freinberg, Austria*

DOI 10.3217/978-3-99161-089-2-030, license CC BY 4.0

ABSTRACT

Additive manufacturing (AM) offers significant design freedom compared to conventional manufacturing methods. This enables the production of complex, topology-optimized metal components. While powder bed processes are well-established for small to medium-sized parts, large-scale applications benefit from directed energy deposition (DED) techniques such as wire-arc directed energy deposition (wa-DED). Despite its potential, limited research addresses topology optimization specifically tailored to the constraints of wa-DED. This study presents a workflow for wa-DED-compatible topology optimization, using a semi-trailer kingpin plate as a demonstrator geometry. All simulations were conducted using Altair OptiStruct. Multiple optimization scenarios were evaluated to compare the impact of different optimization approaches and manufacturing constraints. The most suitable design achieved a 59 % weight reduction compared to the initial design using minimized mass fraction with stress, deformation and draw type constraints. A nonlinear finite element (FE) analysis confirmed the structural integrity of the optimized geometry under relevant load cases. To validate manufacturability, a quarter section of the design was successfully fabricated using wa-DED.

Keywords: wa-DED, topology optimization, FE reanalysis, Altair Optistruct

INTRODUCTION

With a share of 49 %, road transport accounts for the largest portion of total freight transport in the European Union (EU) [1]. It is also a major contributor to EU's greenhouse gas emissions. Road freight alone is responsible for 689.8 million tons of CO_2 equivalent, approximately 76.7 % of all transport-related emissions [2]. Reducing vehicle weight is a proven strategy for improving fuel efficiency and lowering emissions. For example, a 27-ton truck can save 0.05 l/100 km for every 100 kg of weight reduction [3]. Assuming a diesel price of 1.54 € per Liter [4], a trailer weight of 6000 kg [5] and an annual travelling distance of

100000 km, a 25 % reduction in trailer weight can lead to annual fuel cost savings of approximately 1155 €. Besides environmental impact, weight reduction also offers logistical benefits. Regulations limit the total allowable trailer weight. For example, a three-axle trailer forming part of a vehicle combination is restricted to 24 tons [6]. Thus, reduced trailer weight also leads to increased load capacity, thereby improving overall efficiency. However, achieving significant weight reduction without compromising performance is a complex design task.

Numerical methods, such as topology optimization, can assist in this process. Topology optimization is used to determine the optimal material distribution within a given design space by minimizing an objective function F while satisfying predefined constraints [7]. Several case studies have demonstrated the effectiveness of such methods in reducing the weight of truck trailer components with reported savings ranging from 14 % to 29 % [8–10]. The weight reduction of 29 % was achieved through the combined application of topology and thickness optimization [8].

Combining topology optimization with additive manufacturing (AM) enables the full potential of both technologies [11]. In particular, the increased design freedom offered by AM allows for significant additional weight reductions. The selection of an appropriate AM process depends on several factors such as the component size and its material. Wire arc directed energy deposition (wa-DED) is an AM process well suited for producing large metallic components such as those used in truck trailers. Wa-DED uses an electric arc in combination with wire feedstock [12]. This enables the near-net-shape fabrication of metallic components through robot-controlled process movement. For steel, deposition rates can reach up to 10 kg/h [13]. Compared to laser powder bed fusion, wa-DED offers lower investment and operating costs [14]. Although there is extensive research on topology optimization for powder bed processes [15-17] studies specifically focusing on wa-DED remain limited. However, few existing case studies show promising results. In the case of an aeronautical fastening component, the combination of wa-DED and topology optimization enabled a 31 % weight reduction [18]. Additional research has explored the use of wa-DED in the construction sector producing optimized structural nodes, truss structures and T-joints [19-21].

This work investigates the weight reduction potential achievable by combining topology optimization with wa-DED. A kingpin plate for semi-trailers, sometimes also referred as a skid plate, is used as a demonstrator geometry. Fig. 1 shows the S355 steel kingpin plate used in this study. Its primary function is to provide a secure connection between the tractor and the trailer. The flat surface of the kingpin plate transfers vertical loads from the trailer to the tractor, while the kingpin itself locks into the fifth wheel coupling, allowing only rotational movement during turns. The kingpin is mounted to a separate base plate, designated as the retention plate. This retention plate is welded onto the kingpin plate, and the kingpin is attached to it using bolts.

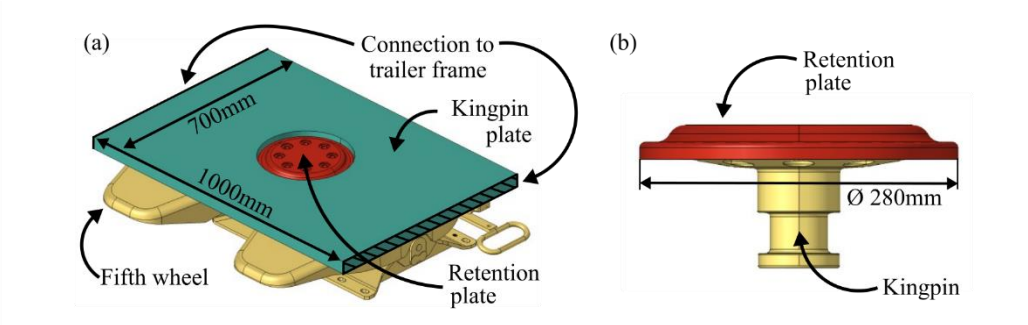

Fig. 1 Fifth wheel coupling (a) assembly of all components (b) assembly of kingpin and retention plate

DESIGN AND BOUNDARY CONDITIONS USED FOR TOPOLOGY OPTIMIZATION

Topology optimization involves numerous iterative solution cycles to achieve an optimal material distribution. To improve computational efficiency, the design space was restricted to a 40 mm thick steel plate with dimensions of 1000 mm × 700 mm. Excluding surrounding components not only reduced computational effort but also enabled the use of global stress constraints. The simplified model is shown in Fig. 2. As a predefined design requirement, the wa-DED structure was embedded between two 6 mm thick steel plates. This configuration creates a closed structure that helps prevent dirt and debris accumulation. In the finite element (FE) model, the plates were represented using first order 2D quadrilateral shell elements with four nodes (CQUAD4), each with an element size of 5 mm. The 28 mm thick optimization region was modelled using first order 3D hexahedral solid elements with eight nodes (HEX8). As for the shells, the element size was set to 5 mm. Shell and solid elements were connected via shared nodes to ensure continuity and avoid contact definitions. To maintain a closed geometry, outer elements were excluded from the design space.

Four load cases were considered. Braking and cornering (in two directions) with loads of 120 kN, and acceleration with loads of 60 kN. The forces were applied using an RBE3 element. Additionally, a distributed surface load of 120 kN was applied to the fifth-wheel contact area to represent trailer weight and payload. As shown in Fig. 2, the steel plate's connection to the trailer was modelled using fixed nodes (locked x, y, and z directions) in the weld seam area. During optimization, linear-elastic material properties were assumed for S355 steel, using a Young's modulus of 210000 N/mm² and a Poisson's ratio of 0.3.

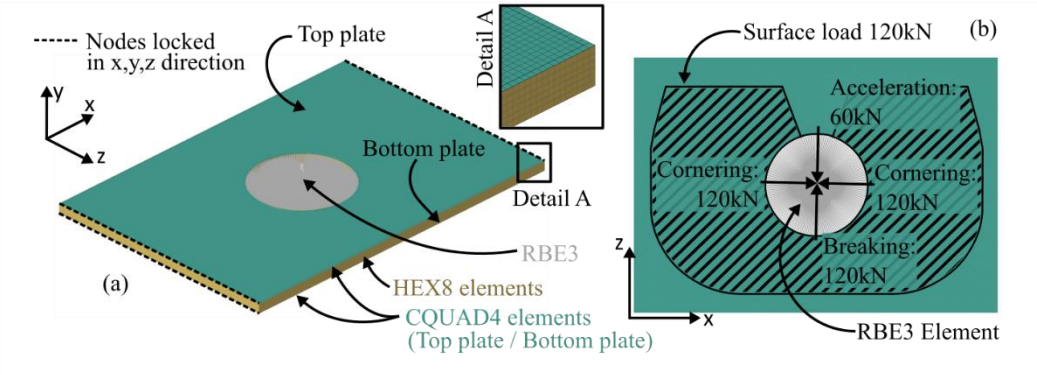

Fig. 2 FE model for topology optimization (a) isometric view (b) bottom view

TOPOLOGY OPTIMIZATION

All simulations in this study were performed using Altair OptiStruct. Topology optimization was carried out using the Solid Isotropic Material with Penalization (SIMP) method [22]. In SIMP, element density is treated as the design variable, and a nonlinear relationship between density and stiffness is applied to drive the solution toward discrete, manufacturable designs.

TOPOLOGY OPTIMIZATION PROBLEM SETUP

Several optimization problem formulations were considered for the kingpin plate [22]. A common approach is to minimize the compliance with constrained volume or mass fraction. Compliance is the inverse of a structure's stiffness [23]. Thus, minimizing the compliance promotes stiffness maximization. Volume fraction describes the ratio between the proposed volume and the original [24]. For example, a volume fraction of 25 % means that only 25 % of the material remain after topology optimization. When working with OptiStruct mass fraction is similar to volume fraction, with the key difference being that mass fraction also considers the non-design mass, while volume fraction only accounts for the design volume [25]. Mass or volume fraction can be used not only as a constraint in optimization but also as an objective function to be minimized, with additional constraints applied to displacements and stresses. Altair OptiStruct supports two types of stress constraints [22]. The first considers global von Mises stress across the entire model, including non-design regions. This method converges quickly, applies stress filtering, and disregards local stress concentrations. The second allows more detailed, component- and subcase-specific definitions of stress types, but often results in slower convergence. Specifications provided by the fifth wheel manufacturer limited the maximum deflection of the bottom plate to ±2 mm. For safety reasons, the maximum stress should not exceed 150 MPa thus ensuring a safety factor greater than two. Based on these criteria, an optimization problem was formulated to minimize mass while

constraining displacements and stress. Additional studies were conducted using increased load values in place of explicit stress constraints. Furthermore, the objective function was modified to minimize compliance, while maintaining constraints on volume and displacement. The resulting designs were compared to identify the most suitable variant for wa-DED manufacturing.

MANUFACTURING CONSTRAINTS

Altair OptiStruct offers a range of manufacturing constraints to guide the generation of feasible, production-ready designs [26]. Since there are currently no wa-DED specific constraints available, existing ones tailored for other manufacturing processes must be applied instead. Extrusion and draw direction constraints were identified as the most suitable options for achieving a wa-DED manufacturable kingpin plate design.

Fig. 3 shows optimization results using different manufacturing constraints. All simulations were conducted using compliance minimization with a constrained mass fraction of 20 %. To better illustrate the effects of the constraints, the top and bottom shell elements were excluded from the design. Without manufacturing constraints, the resulting geometry is highly complex and not suitable for production via wa-DED. The extrusion constraint enforces a uniform cross-sectional profile along a specified direction, while the draw direction constraint also requires a direction but allows for decreasing cross-sectional areas. Originally developed for casting, the draw constraint also includes a Stamp option, which limits the result to a 2D shell-like geometry. This option was not used, as the kingpin plate must maintain flat surfaces on both the top and bottom to ensure proper assembly.

Additional manufacturing constraints can be applied to control the minimum and maximum member sizes within the design space. This is particularly important for wa-DED, where excessive material accumulation may lead to localized heat buildup and thermal distortion. Such effects are especially critical when using thin substrate plates, such as the 6 mm steel plates employed in this study. However, in OptiStruct, the maximum member size must be at least six times the average mesh size. To achieve a desired layer width between 6 and 9 mm, a mesh size of approximately 1.5 mm would be required. Using a mesh size of 1.5 mm would result in excessively long simulation times and reduced computational efficiency. Therefore, no member size constraints were imposed on the design.

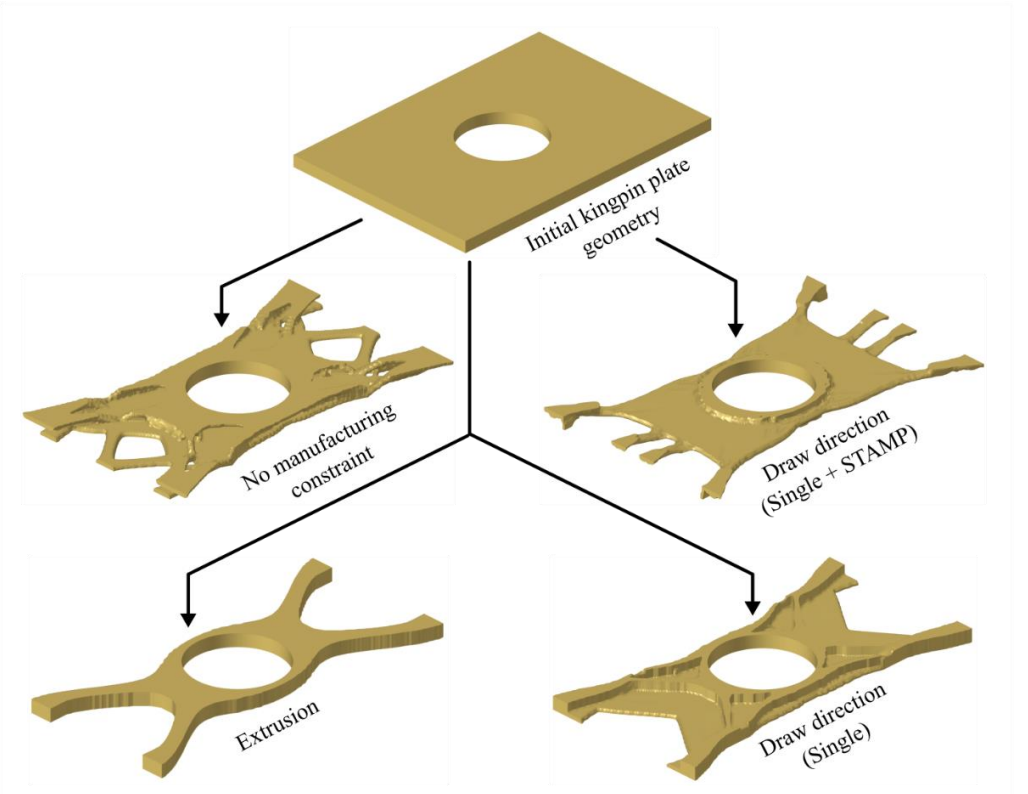

Fig. 3 Optimization of the initial king plate geometry using different manufacturing constraints

Except for the unconstrained case, all configurations shown in Fig. 3 are considered manufacturable using wa-DED. Based on these findings, subsequent optimization studies used the draw direction constraint (without the Stamp option), as it more closely reflects wa-DED capabilities. Unlike extrusion, wa-DED does not require a constant cross-section throughout the building height, making the draw direction constraint a better fit for the process.

FE REANALYSIS

During topology optimization, only the solid and shell elements representing the kingpin plate were considered. To assess the structural behaviour under more realistic boundary conditions, a FE reanalysis was performed on the optimized design. The corresponding FE model is shown in Fig. 4. Compared to the simplified model used in Fig. 2, the updated model includes additional components such as the fifth wheel, the retention plate, and the kingpin, as well as their interactions. Surface loads were applied in the regions where the kingpin plate is later connected to the trailer frame. As in the optimization phase, four load cases were simulated,

covering acceleration, cornering, and braking scenarios. The total applied forces in each case matched those used in the optimization setup (see Fig. 2). Fig. 4 (a) schematically illustrates the force directions for the braking load case.

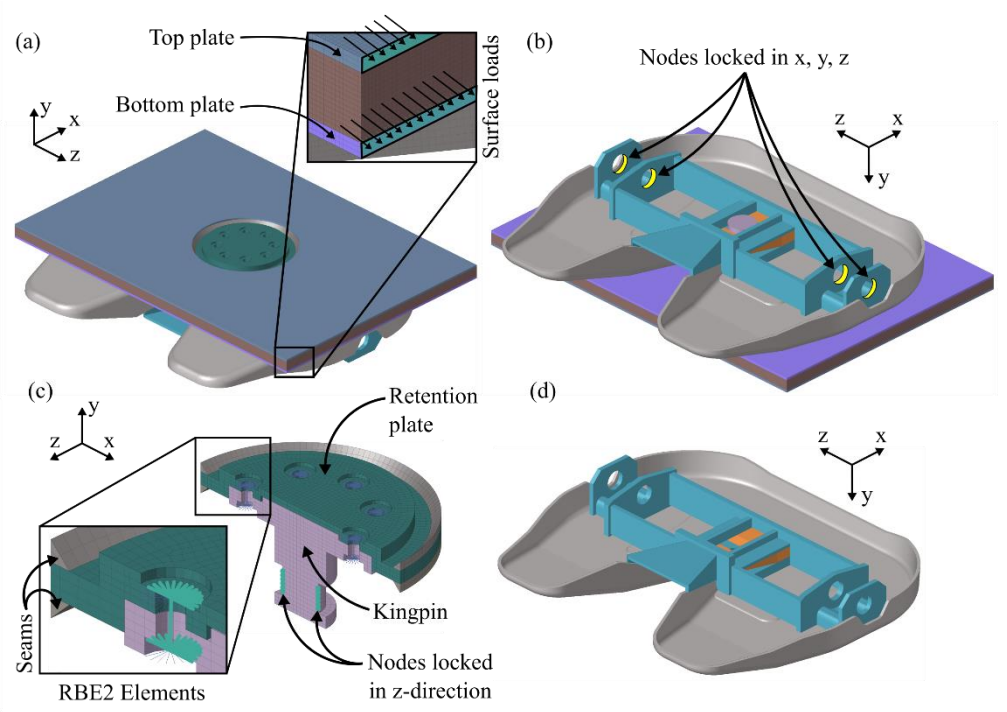

Fig. 4 Model for FE reanalysis (a) surface load orientation (braking load case) (b) locked fifth wheel nodes (c) constrained kingpin nodes and RBE2 elements for retention plate connection (braking load case) (d) fifth wheel components connected using freezing contact

To fully constrain the system, the nodes at the bolt holes, where the fifth wheel attaches to the tractor, were fixed in the x, y, and z directions (Fig. 4 (b)). Contact interactions between the fifth wheel, kingpin plate, and kingpin were defined assuming a friction coefficient of 0.1 for the lubricated steel on steel contact. To prevent undesired rotation of the kingpin plate, selected nodes on the kingpin were constrained in either the x or z direction, depending on the load case (Fig. 4 (c)). The wa-DED structure and the top and bottom steel plates were meshed using 2 mm elements, while 4 mm elements were used for the fifth wheel and the kingpin. RBE2 elements were employed to connect the kingpin to the retention plate. All fifth-wheel components shown in Fig. 4 (d) were connected using freezing contact, thereby enforcing zero relative motion between the contact faces. The weld seams between the kingpin plate and the retention plate were modelled with a throat thickness (a-dimension) of 7 mm and connected via freezing contact.

RESULTS

Fig. 5 illustrates the final design of the kingpin plate, which was developed using a single draw-type manufacturing constraint combined with defined limits for stress and deformation. Compared to the initial design using a 40 mm thick steel plate with a weight of 200 kg the mass was reduced by 59 %.

During fabrication, the wa-DED structure is deposited directly onto the substrate plate. In the regions along the four outer edges and the inner circular recess, the layer width is increased by 3 mm to allow for subsequent machining. These areas, indicated by hatching in Fig. 5, are subjected to subtractive post-processing to meet dimensional and surface quality requirements. In addition to the outer contours, the top surface is also machined to ensure a flat and uniform bonding area for the attachment of the top plate.

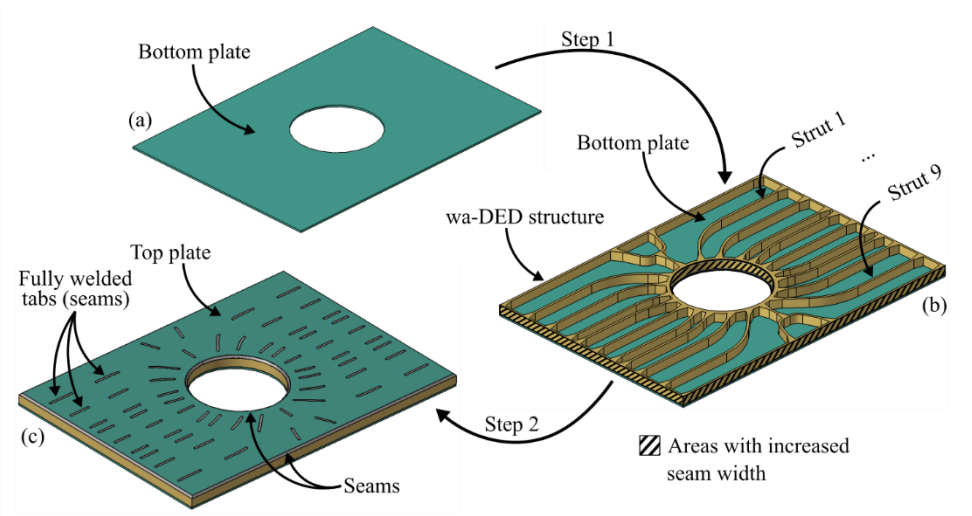

Fig. 5 Manufacturing steps for the wa-DED optimized kingpin plate (a) bottom plate (b) wa-DED structure on bottom plate with highlighted machining surfaces (c) final design including top plate

Following the machining process, the top plate is positioned and joined to the wa-DED structure. This is accomplished by fully welding the pre-cut tabs in the top plate to the underlying additively manufactured features. Additional fillet welds are applied around the kingpin hole and along the side interfaces to ensure adequate structural performance and reliable load transfer.

A comparative evaluation of three different topology optimization problem setups guided the selection of the final kingpin plate geometry. Fig. 6 presents the results for each setup. All optimization runs incorporated a single draw-type manufacturing constraint to ensure compatibility with wa-DED fabrication requirements. Variants 1 and 2 were formulated to minimize mass fraction while imposing a maximum allowable deformation of ±2 mm.

In Variant 1, an initial optimization was conducted with only the deformation constraint. The resulting geometry served as a non-design space for the subsequent refinement step, referred to as Variant 1 (b). In this step, a global stress constraint was introduced to limit the maximum stress to 150 MPa and avoid critical stress concentrations. While the optimized geometry met the strength and deformation requirements, issues emerged during the subsequent finite element reanalysis (FEA). In the topology optimization phase, all nodes at the interface between the wa-DED structure and the top plate were treated as fully connected. However, in the reanalysis, only nodes located in the actual weld regions, specifically at the fully welded tabs shown in Fig. 5, were modelled as shared. During topology optimization, it was not possible to consider shared nodes only in the actual weld regions, since their definition is based on the geometry resulting from the optimization process. To mitigate the stress concentrations observed in the reanalysis, the number of wa-DED struts was increased. It was found that a configuration with at least seven struts effectively reduced stress in the welded connection zones to acceptable levels. This was achieved by iteratively reducing the maximum allowable stress constraint, with a limit of 120 MPa yielding the desired structural layout.

Variant 2 retained the ±2 mm deformation constraint but followed a different approach to reduce stress concentrations. Instead of applying an explicit stress constraint, the applied loads were scaled by a factor of 1.65 during optimization to indirectly encourage the formation of a seven-strut configuration similar to Variant 1 (b). The scaling factor was determined through iterative refinement.

In Variant 3, the objective function was changed to compliance minimization, with constraints on volume and displacement. With a total of 32 iterations and a CPU time of 35 minutes, the computational costs are low compared to Variants 1 and 2. Although this setup yields a structurally valid solution quickly, it leads to significant material accumulation, making the design unsuitable for wa-DED manufacturing. Consequently, Variant 3 was excluded from further consideration.

Variants 1 and 2 were translated into manufacturable CAD models using Autodesk Inventor. The entire structure was designed such that the wa-DED layers have a width of 7 mm. Exceptions include the inner connection to the kingpin plate, where a 12 mm layer width was applied, and the strut interfaces, where the width was increased to 23 mm to enlarge the bonding surface and reduce stress concentrations.

The final CAD representations of Variants 1 (b) and 2 are shown in Fig. 7. For the final design based on Variant 1 (b), the small struts adjacent to struts 3 and 5 were treated as separate members, resulting in a total of nine struts. Although this configuration weighs 82 kg (1 kg more than Variant 2) it was selected as the final design. The decision was based on its reduced number of intersections. While wa-DED is capable of manufacturing complex three-dimensional geometries, intersections in particular are associated with an increased risk of defects, making a design with fewer such features preferable. In Variant 1 (b), intersections occur only at the four outer edges and at the inner circular recess, whereas Variant 2 additionally exhibits intersections between the individual struts.

The computation time for Variant 2, 1 hour and 42 minutes, is shorter than that of Variant 1 (a and b), which requires 2 hours and 19 minutes. However, this difference was not considered in the decision-making process, as the focus of the study is on the manufacturability of the structure.

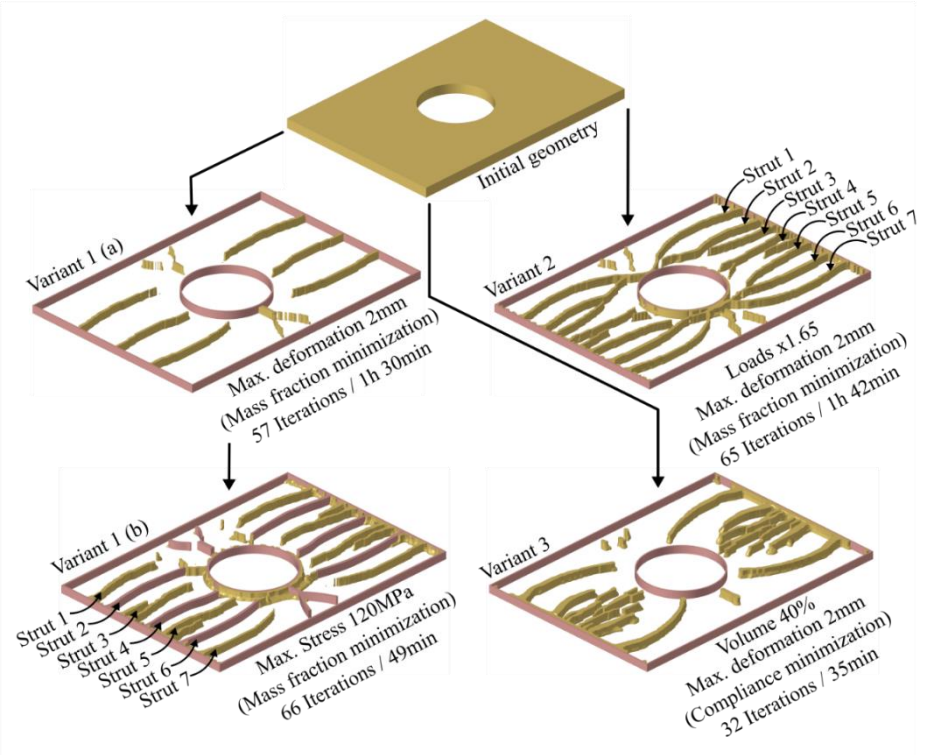

Fig. 6 Topology optimized designs of the initial kingpin plate geometry obtained using different optimization objectives and constraints, along with the corresponding computational costs (top and bottom plates not shown)

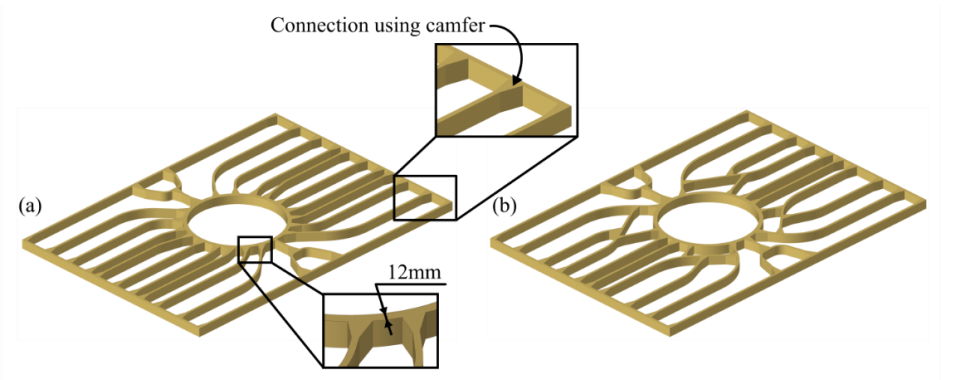

Fig. 7 Processed CAD models of the optimized structures (a) Variant 1: deformation and stress constraint (b) Variant 2: increased loads and deformation constraint

FE REANALYSIS

The results of the FE reanalysis are presented in Fig. 8 to Fig. 11. In contrast to the topology optimization model, where all nodes at the interface between the wa-DED structure and the top plate were shared, the reanalysis model applies shared nodes only within the defined weld seam areas and the regions of the fully welded tabs, as indicated in Fig. 5. All four load cases were evaluated.

Fig. 8 shows the deformation in the y-direction, with the maximum deformation occurring under the braking load case, ranging from +0.73 mm to -1.5 mm. These values remain within the allowable limit of ±2 mm, thus fulfilling the displacement requirement. For the cornering load cases, the deformation patterns exhibit asymmetry with respect to the xy-plane. This behaviour results from the asymmetric contact geometry between the kingpin and the fifth wheel, as illustrated in Fig. 9. Fig. 10 presents the von Mises stress distribution across all load cases. The highest stress condition, 242 MPa, occurs in the cornering load case with force applied in the negative z-direction. Compared to the material's yield strength of 355 MPa, this results in a safety margin that is too low.

When isolating elements with stress values above 150 MPa (Fig. 11), it becomes apparent that the highest stresses are located in the regions of the fully welded tabs where the substrate is connected to the top plate via shared nodes. These stress concentrations are most likely numerical artifacts and are not expected to occur in the actual component. Additional stress concentrations above 150 MPa are observed at the bottom of the wa-DED structure, where it interfaces with the bottom plate. These are likely caused by contact interactions between the fifth wheel edge and the bottom plate. However, the stress levels in this region remain below the peak value of 242 MPa.

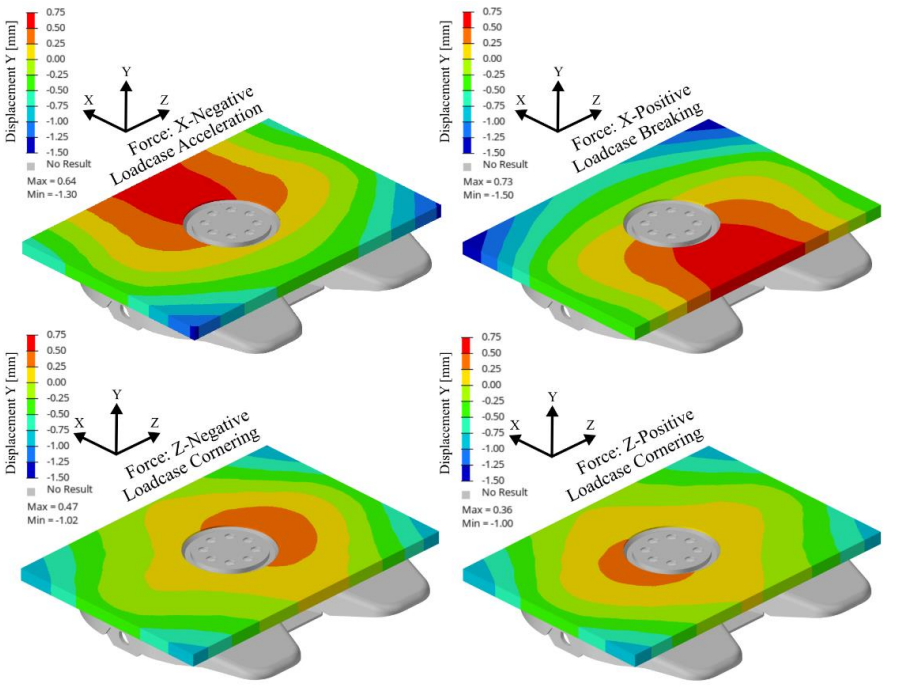

Fig. 8 FE reanalysis (y-direction displacements) for the four load cases: acceleration, braking, and both cornering cases

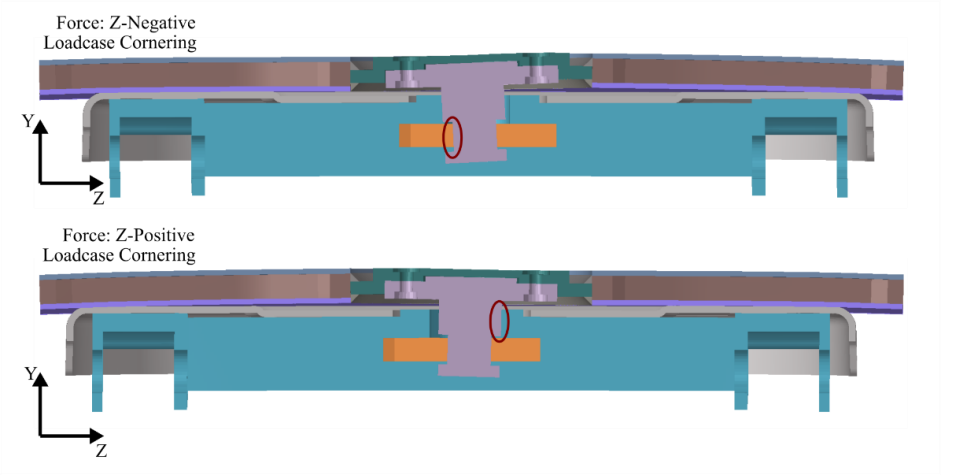

Fig. 9 FE reanalysis (kingpin contact faces for cornering load cases marked in red / displacement scale factor 10)

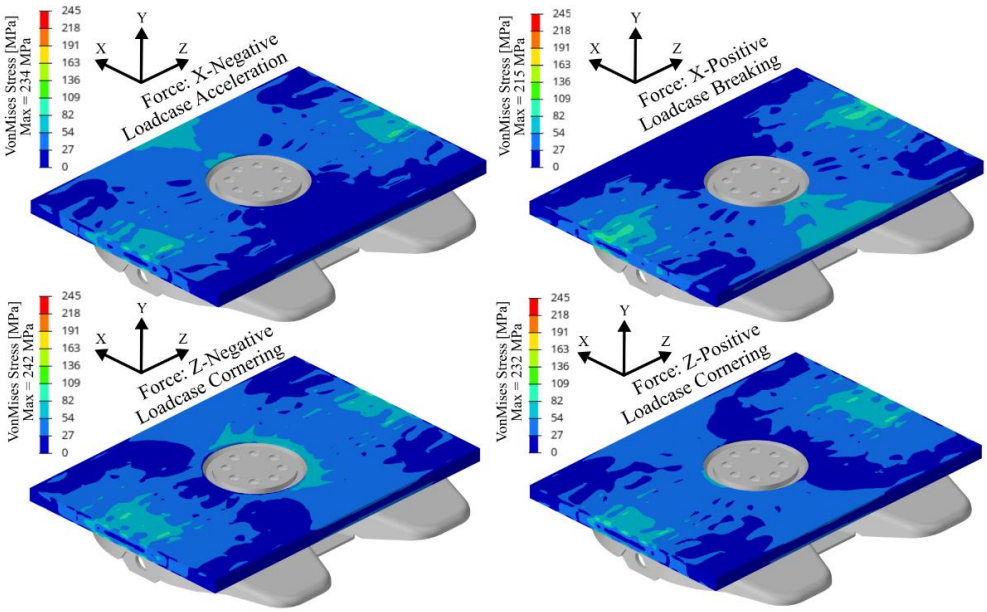

Fig. 10 FE reanalysis (VonMises Stresses) for the four load cases: acceleration, braking, and both cornering cases

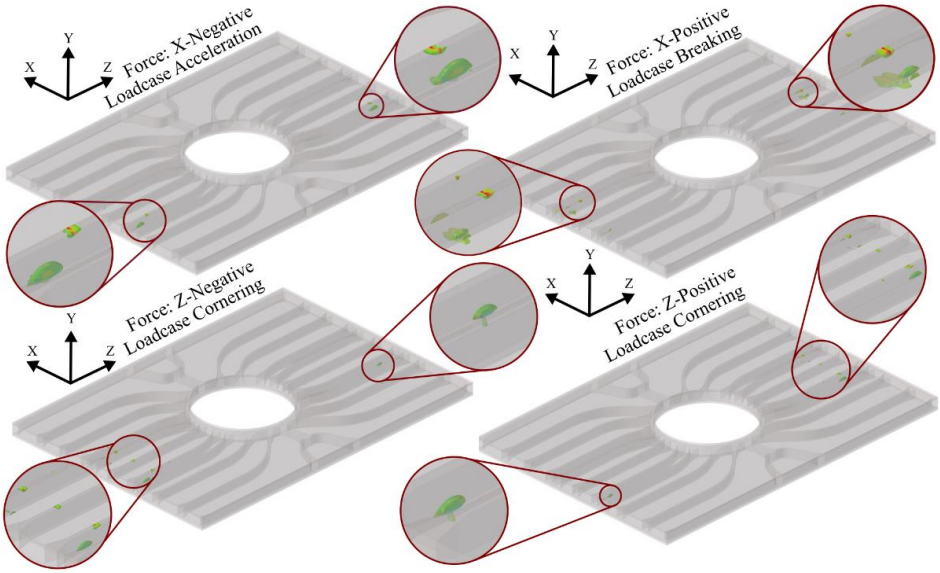

Fig. 11 FE reanalysis (regions with VonMises Stress > 150MPa) for the four load cases: acceleration, braking, and both cornering cases

WA-DED MANUFACTURING

To validate the manufacturability of the optimized design using wa-DED, a quarter section of the structure was fabricated. An image of the manufactured section is shown in Fig. 12. The wa-DED system consists of a KUKA KR 300 R2700-2 industrial robot in combination with a Fronius iWave 500i AC/DC power source. All wa-DED structures were deposited using Fronius CMT Additive Pro process and a Böhler EMK-6 wire with a diameter of 1.2 mm. The flow rate of the M12 shielding gas was set to 15 L/min.

A constant travel speed of 12 mm/s was maintained throughout the build-up. To achieve the required layer width, a rectangular weaving pattern was employed. The weave amplitude was automatically adjusted to the desired layer width using the ModuleWorks LAM module within Mastercam software. Robot offline programming and post processing was carried out in Robotmaster. All CAM software solutions were supplied by robotized rm systems. To promote adequate fusion at intersecting regions, the heat input was locally increased by applying Additive Pro power correction and adjusting the wire feed rate.

During the build-up, the substrate was clamped to a tilting/rotary table equipped with internal cooling channels for active temperature control. The temperature of the circulating fluid was regulated using a Robamat heating and cooling unit. With this setup, the S355 substrate plate was preheated to 65 °C. Once the build-up process started, the coolant setpoint was reduced to 40 °C to prevent heat accumulation in the welding table and thereby minimize dwell times. Due to the large thermal mass of the work table, this adjustment did not result in an immediate reduction of the substrate temperature. Instead, the table responded gradually to the changed coolant temperature, providing a controlled cooling effect.

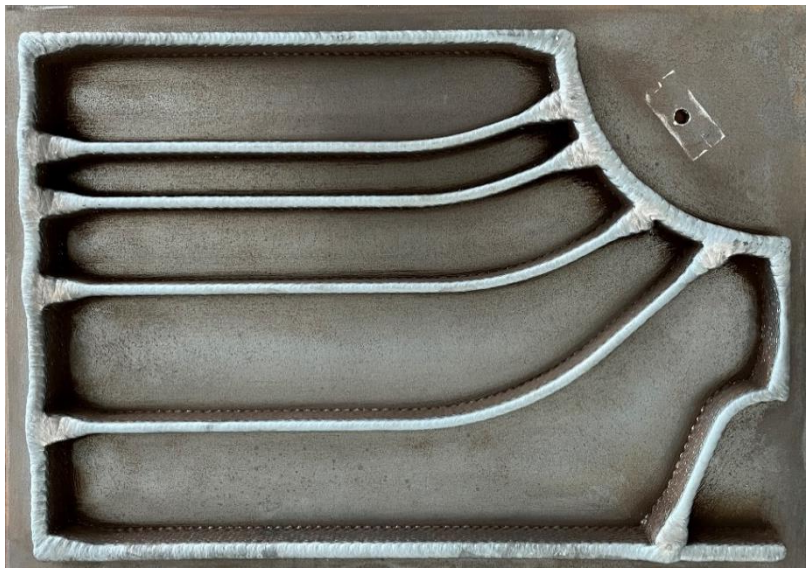

Fig. 12 Quarter section demonstrator manufactured via wa-DED

To further reduce dwell times, the interlayer temperature was set to approximately 150 °C. In contrast to lower interlayer temperatures, such as 100 °C, this value helps to maintain short dwell times even in the upper layers, while also ensuring that the material achieves the required yield strength of 355 MPa [27-28]. The measurement of the interlayer temperature was carried out manually using a Type K surface probe.

Although a constant interlayer temperature was maintained, a gradual reduction in wire feed speed was required with an increasing number of layers. The first layer was deposited using a wire feed speed of 4.7 m/min. In subsequent layers the wire feed speed was gradually decreased from 4.0 m/min to 3.5 m/min. This adjustment was required because heat dissipation into the substrate becomes less effective as the build height increases. Moreover, despite active cooling, the global component temperature rises continuously from the initial 60 °C with increasing layer number. Applying this thermal strategy resulted in a total fabrication time of approximately 4.5 hours for the quarter section.

SUMMARY AND OUTLOOK

This study presents a comprehensive investigation into the potential of combining topology optimization with wa-DED to design a lightweight, structurally efficient kingpin plate for semi-trailers. The goal was to reduce weight without compromising performance while ensuring manufacturability. Various topology optimization strategies were explored, including mass fraction minimization under stress and deformation constraints and compliance minimization under volume and deformation restrictions. Among the evaluated approaches, the most promising results were obtained using a two-step mass fraction minimization strategy which incorporated both deformation and global stress constraints alongside a draw-direction manufacturing constraint. This configuration yielded a structurally valid design with improved stress distribution, reduced complexity, and a final mass of 82 kg, resulting in a 59 % weight reduction compared to the original 200 kg steel plate.

A detailed finite element reanalysis incorporating realistic boundary conditions, contact interactions, and weld seam modelling confirmed that the optimized structure met all functional requirements. Displacements remained within the allowable ±2 mm threshold across all load cases. Local stress concentrations with a maximum value of 242 MPa remain below the materials yield strength but exceed the defined limit of 150 MPa. The highest stress concentrations occurring in the area of the shared nodes between the substrate and the top plate are assumed to be caused by numerical effects. They are not expected to affect the structural performance. The simulation results suggest that the optimized design maintains an acceptable safety margin under all critical loading scenarios.

To validate the practical feasibility of the proposed design, a quarter-section of the optimized structure was successfully manufactured using a robotic wa-DED system. This step confirmed that the design is compatible with current AM capabilities. Preheating and cooling strategies were employed to ensure proper material quality while reducing dwell times.

To ensure suitability for real-world applications, future studies should address more complex loading conditions and include a detailed evaluation of the material’s fatigue

performance. In addition, it would be important to assess how accurately FEM simulations can capture the mechanical behaviour of wa-DED structures in the as-built condition.

APPENDICES AND ACKNOWLEDGEMENTS

This research was funded by the federal state of Upper Austria in the project “GEPROBA - Gesteigerte Prozess- und Bauteilperformance durch neue Fertigungsmöglichkeiten für eMobilitäts-Anwendungen” (grant no. 901696) administered by Austrian Funding Agency (FFG) within the framework “Future Mobility”. The authors thank the project partners for the collaborative work.

References

[1] J. BARAN and A. K. GÓRECKA: ‘Economic and environmental aspects of inland transport in EU countries’, *Economic Research-Ekonomska Istraživanja*, vol. 32, pp. 1037-1059, 2019, doi: 10.1080/1331677X.2019.1578680.

[2] J. DOMAGAŁA and M. KADŁUBEK: ‘Economic, Energy and Environmental Efficiency of Road Freight Transportation Sector in the EU’, *Energies*, vol. 16, 2023, doi: 10.3390/en16010461.

[3] RICARDO-AEA: *Light weighting as a means of improving Heavy Duty Vehicles’ energy efficiency and overall CO2 emissions: Heavy Duty Vehicles Framework Contract – Service Request 2*, 2015.

[4] *Weekly Oil Bulletin*, accessed: Jul. 10, 2025. [Online]. Available: https:/energy.ec.europa.eu/data-and-analysis/weekly-oil-bulletin_en

[5] WILHELM SCHWARZMÜLLER GMBH, accessed: Jul. 10, 2025. [Online]. Available: https:/schwarzmueller.com/de/fahrzeuge/plateau-fahrzeuge/plateausattel-standard/3-achs-schiebeplanen-plateausattel/

[6] EUROPEAN PARLIAMENT: *Road vehicles: maximum weights and dimensions: P9_TA(2024)0126*, 2024.

[7] O. SIGMUND and K. MAUTE: ‘Topology optimization approaches’, *Struct Multidisc Optim*, vol. 48, pp. 1031-1055, 2013, doi: 10.1007/s00158-013-0978-6.

[8] G.-W. JANG, M.-S. YOON and J. H. PARK: ‘Lightweight flatbed trailer design by using topology and thickness optimization’, *Struct. Multidisc. Optim.*, vol. 41, pp. 295-307, 2010, doi: 10.1007/s00158-009-0409-x.

[9] J. GALOS and M. SUTCLIFFE: ‘Material Selection and Structural Optimization for Lightweight Truck Trailer Design’, *SAE International Journal of Commercial Vehicles*, 2020, doi: 10.4271/02-12-04-0022.

[10] D. GAO, J. MA, H. ZHENG, M. ZHANG and J. ZHAO: ‘Optimal Design of Frame Structure of Center Axle Trailer Under Heavy Load Conditions’, pp. 201-219, doi: 10.1007/978-981-97-1876-4_16.

[11] J. ZHU, H. ZHOU, C. WANG, L. ZHOU, S. YUAN and W. ZHANG: ‘A review of topology optimization for additive manufacturing: Status and challenges’, *Chinese Journal of Aeronautics*, vol. 34, pp. 91-110, 2021, doi: 10.1016/j.cja.2020.09.020.

[12] K. TREUTLER and V. WESLING: ‘The Current State of Research of Wire Arc Additive Manufacturing (WAAM): A Review’, *Applied Sciences*, vol. 11, 2021, doi: 10.3390/app11188619.

[13] C. WANG ET AL.: ‘A novel cold wire gas metal arc (CW-GMA) process for high productivity additive manufacturing’, *Additive Manufacturing*, vol. 73, 2023, doi: 10.1016/j.addma.2023.103681.

[14] R. LACHMAYER, R. B. LIPPERT and S. KAIERLE: *Additive Serienfertigung*. Berlin, Heidelberg: Springer Berlin Heidelberg, 2018.
[15] T. MIKI: 'Self-support topology optimization considering distortion for metal additive manufacturing', *Computer Methods in Applied Mechanics and Engineering*, vol. 404, 2023, doi: 10.1016/j.cma.2022.115821.
[16] M. ZHOU, Y. LIU and Z. LIN: 'Topology optimization of thermal conductive support structures for laser additive manufacturing', *Computer Methods in Applied Mechanics and Engineering*, vol. 353, pp. 24-43, 2019, doi: 10.1016/j.cma.2019.03.054.
[17] N. IYER ET AL.: 'PATO: Producibility-Aware Topology Optimization Using Deep Learning for Metal Additive Manufacturing', *Int. J. Interact. Des. Manuf.*, vol. 18, pp. 7459-7476, 2024, doi: 10.1007/s12008-024-01905-z.
[18] F. VEIGA, A. SUÁREZ, E. ALDALUR, I. GOENAGA and J. AMONDARAIN: 'Wire Arc Additive Manufacturing Process for Topologically Optimized Aeronautical Fixtures', *3D Printing and Additive Manufacturing*, early access. doi: 10.1089/3dp.2021.0008.
[19] J. REIMANN ET AL.: 'Production of Topology-optimised Structural Nodes Using Arc-based, Additive Manufacturing with GMAW Welding Process', *J. Civ. Eng. Constr.*, vol. 10, pp. 101-107, 2021, doi: 10.32732/jcec.2021.10.2.101.
[20] J. YE, P. KYVELOU, F. GILARDI, H. LU, M. GILBERT and L. GARDNER: 'An End-to-End Framework for the Additive Manufacture of Optimized Tubular Structures', *IEEE Access*, vol. 9, pp. 165476-165489, 2021, doi: 10.1109/ACCESS.2021.3132797.
[21] K. MONTEIRO, C. ZHU, A. F. SANTOS, L. S. DA SILVA and T. TANKOVA: 'Integrated topological optimization and production of an additively manufactured steel T-joint: A case study', *Structures*, vol. 74, 2025, doi: 10.1016/j.istruc.2025.108511.
[22] ALTAIR LEARNING: *OptiStruct for Optimization Basics*, accessed: Aug. 23, 2025. [Online]. Available: https://learn.altair.com/ (restricted access)
[23] D. V. N. LUCA: 'Optimization of Varying Orientation of Continuous Fiber Direction and Its Applications to New Methods of Additive Manufacturing', *RDMS*, 2018, doi: 10.31031/RDMS.2018.03.000559.
[24] M. SOTOLA, P. MARSALEK, D. RYBANSKY, M. FUSEK and D. GABRIEL: 'Sensitivity Analysis of Key Formulations of Topology Optimization on an Example of Cantilever Bending Beam', *Symmetry*, vol. 13, 2021, doi: 10.3390/sym13040712.
[25] ALTAIR: *Design Optimization Responses*, accessed: Aug. 24, 2025. [Online]. Available: https:/help.altair.com/2023.1/hwsolvers/os/topics/solvers/os/responses.htm
[26] ALTAIR: *Topology Optimization Manufacturability*, accessed: Jun. 20, 2025. [Online]. Available: https:/2021.help.altair.com/2021/hwsolvers/os/topics/solvers/os/mfg_topology_opt_intro_c.htm #mfg_topology_opt_intro_c
[27] B. TURGUT, U. GÜROL and R. ONLER: 'Effect of interlayer dwell time on output quality in wire arc additive manufacturing of low carbon low alloy steel components', *Int. J. Adv. Manuf. Technol.*, vol. 126, 11-12, pp. 5277–5288, 2023, doi: 10.1007/s00170-023-11481-3.
[28] G. D. C. LOPES, D. F. FILHO and V. A. FERRARESI: 'Effect of interlayer temperature and cold wire addition in Wire Arc Additive Manufacturing on carbon steel', *Procedia Computer Science*, vol. 232, pp. 544-553, 2024, doi: 10.1016/j.procs.2024.01.054.